EUROFUSION WPPFC-PR(16) 14725

P Tolias et al.

Experimental validation of the analytical model for tungsten dust-wall mechanical impacts incorporated in the MIGRAINe dust dynamics code

Preprint of Paper to be submitted for publication in
22nd International Conference on Plasma Surface Interactions
in Controlled Fusion Devices (22nd PSI)

This work has been carried out within the framework of the EUROfusion Consortium and has received funding from the Euratom research and training programme 2014-2018 under grant agreement No 633053. The views and opinions expressed herein do not necessarily reflect those of the European Commission.

Experimental validation of the analytical model for tungsten dust - wall mechanical impacts incorporated in the MIGRAINe dust dynamics code

P. Tolias,[1] S. Ratynskaia,[1] A. Shalpegin,[2] L. Vignitchouk,[1] F. Brochard,[2] M. De Angeli[3] and H. van der Meiden[4]

[1] *Space and Plasma Physics - KTH Royal Institute of Technology, Teknikringen 31, 10044 Stockholm, Sweden*
[2] *Université de Lorraine, Institut Jean Lamour, UMR 7198 CNRS, F-54506 Vandoeuvre-lés-Nancy, France*
[3] *Istituto di Fisica del Plasma - Consiglio Nazionale delle Ricerche, via Cozzi 53, 20125 Milan, Italy*
[4] *FOM Institute DIFFER, Dutch Institute For Fundamental Energy Research, Eindhoven, The Netherlands*

Abstract

Mechanical dust-wall collisions are unavoidable in fusion devices and their accurate modelling is essential for the understanding of dust transport. The MIGRAINe dust dynamics code features analytical models addressing all facets of dust-surface impacts, some aspects of which have not been experimentally validated thus far. Dedicated dust injection experiments have been carried out in Pilot-PSI resulting to the visualization of *in-plasma* tungsten dust-surface impacts with an unprecedented resolution. They allowed for a calibration of key quantities of the MIGRAINe impact model.

1. Introduction

Dust-wall impacts are an unambiguous constituent of dust dynamics in fusion devices owing to the curved ion flow and inertial effects [1, 2]. They have been recently demonstrated to be crucial for long distance W dust transport [3]. The low speed regime is most relevant for mechanical collisions of dust with plasma-facing-components, given the impact speeds predicted by codes and measured by cameras [4, 5]. It is characterized by energy losses due to adhesive work, plastic deformation and frictional dissipation.

MIGRAINe is the only dust dynamics code that incorporates analytical models addressing all facets of dust-wall collisions [6]. The treatment of spherical dust - planar surface collisions consists of two deterministic models for the normal and tangential components of the impact and two probabilistic models for the effects of roughness at the micrometer and nanometer scales [3, 6]. The dependence of the mechanical properties on the bulk dust temperature and size is also taken into account. The normal component is analyzed within the Thornton and Ning approach for elastic-perfectly plastic adhesive spheres (T&N model) [7]. The tangential component is treated by rigid body theory for frictional contacts [8]. Roughness is introduced by randomizing the impact geometry and work of adhesion.

Certain aspects of the MIGRAINe impact model have been identified that require experimental validation. Controlled dust injection experiments were carried out in the Pilot-PSI linear device targeting direct camera visualization of *in plasma* W dust - W surface impacts [9]. Highly resolved measurements up to 6.5 μm/px were possible by utilizing an optical setup that uses fast cameras as a basic microscope [10]. Despite the unavoidable uncertainties, the large impact statistics with such an unprecedented resolution allowed for a calibration of the impact model.

2. Theoretical aspects

Mechanical impacts involve very short-range forces and are instantaneous compared to the time-scales relevant for dust motion. Due to the impulsive nature of the interaction, they are quantified with the aid of restitution coefficients. The impact angle is defined with respect to the surface normal of the planar colliding body. We denote the incident normal (tangential) velocity component with $v_{\rm inc}^{\perp}$ ($v_{\rm inc}^{\parallel}$) and the rebound normal (tangential) velocity component with $v_{\rm reb}^{\perp}$ ($v_{\rm reb}^{\parallel}$), the normal (tangential) restitution coefficient is defined by $e_{\perp} = v_{\rm reb}^{\perp}/v_{\rm inc}^{\perp}$ ($e_{\parallel} = v_{\rm reb}^{\parallel}/v_{\rm inc}^{\parallel}$).

Normal impact component. The analytical T&N model assumes the additivity of dissipation by adhesive work and plastic deformation [7]. The elastic-adhesive part of the impact is treated within the Johnson-Kendall-Roberts (JKR) theory [11] and the elastic-perfectly plastic part of the impact is treated by truncating the Hertzian pressure profile at the limiting contact pressure $p_{\rm y}$. Two characteristic velocities emerge [12]; the adhesive velocity $v_{\rm s}^{\rm adh}$ that is the maximum impact velocity for which an elastic-adhesive impact leads to zero rebound velocity and the yield velocity $v_{\rm y}$ that is the minimum impact velocity for which a pure elastic impact starts to become plastic,

$$v_{\rm s}^{\rm adh} = \frac{\sqrt{3}}{2}\pi^{1/3}\sqrt{\frac{1+6\times 2^{2/3}}{5}}\left(\frac{\Delta\gamma^5}{\rho_{\rm d}^3 E^{*2} R_{\rm d}^5}\right)^{1/6}, \quad (1)$$

$$v_{\rm y} = \frac{\pi^2}{2\sqrt{10}}\left(\frac{p_{\rm y}^5}{\rho_{\rm d} E^{*4}}\right)^{1/2}, \quad (2)$$

where $R_{\rm d}$ is the dust radius, $\rho_{\rm d}$ is the dust mass density, E^* is the reduced Young's modulus, $\Delta\gamma = \gamma_1 + \gamma_2 - \Gamma$ is the work of adhesion with γ_i the surface energy and

Γ the interface energy. Finally, the sticking velocity is defined by $v_\mathrm{s} = v_\mathrm{y}/w_0$, where $0 < w_0 \leq 1$ is the solution of $6\sqrt{3}(1-w^2/6)/5 = (v_\mathrm{s}^\mathrm{adh}/v_\mathrm{y})^2 w^{3/2}(w+2\sqrt{6-w^2}/\sqrt{5})^{1/2}$. The normal restitution coefficient is given by

$$e_\perp^2 = \left\{ \frac{6\sqrt{3}}{5}\left(\frac{v_\mathrm{y}}{v_\mathrm{inc}^\perp}\right)^{1/2}\left[\frac{v_\mathrm{y}}{v_\mathrm{inc}^\perp}+\frac{2}{\sqrt{5}}\sqrt{6-\left(\frac{v_\mathrm{y}}{v_\mathrm{inc}^\perp}\right)^2}\right]^{-1/2} \left[1-\frac{1}{6}\left(\frac{v_\mathrm{y}}{v_\mathrm{inc}^\perp}\right)^2\right] - \left(\frac{v_\mathrm{s}^\mathrm{adh}}{v_\mathrm{inc}^\perp}\right)^2 \right\} \mathrm{H}\left(v_\mathrm{inc}^\perp - v_\mathrm{s}\right) , \quad (3)$$

where H(.) denotes the Heaviside step function. The restitution curve is very sensitive to the limiting contact pressure that is proportional to the material's yield strength σ_y. Finite element modelling of sphere-plane impacts suggests that the ratio lies between 1.6 and 2.8 [13, 14], but even higher values have been experimentally obtained [15]. MIGRAINe currently employs $p_\mathrm{y} = 2.8\sigma_\mathrm{y}$ [6].

Tangential impact component. The application of rigid body theory in the sliding regime results to a simple relation for the tangential restitution coefficient [8]

$$e_\parallel = 1 - \mu\left(v_\mathrm{inc}^\perp / v_\mathrm{inc}^\parallel\right)(1+e_\perp) , \quad (4)$$

where μ is a friction constant. Owing to the difficulty of obtaining reliable experimental values for μ and consistency issues concerning rotational dust dynamics, MIGRAINe currently assumes a frictionless contact $\mu = 0$ [3].

There are no strong theoretical arguments that dictate a unique material-independent value for the ratio $p_\mathrm{y}/\sigma_\mathrm{y}$, whereas the underlying $e_\parallel$ theory can be deemed as oversimplified. It is, thus, important to perform dedicated impact experiments to obtain approximate values for these quantities by comparison with measured restitution curves.

3. Experimental aspects

The experimental methodology comprises of dust injection in the discharge, dust visualization by thermal radiation capture, trajectory reconstruction in the target vicinity, detection of the dust-target impact, determination of the normal and tangential components of the impact and rebound velocities and finally calculation of the normal and tangential restitution coefficients.

Pilot-PSI linear device. The plasma is generated by a cascaded arc source exhausting into a 40 cm diameter vessel and confined by an axial magnetic field. The hydrogen plasma has a Gaussian decaying radial density profile [16]. Essentially, an elongated cylindrical plasma column is formed with a 1 cm diameter and a 54 cm length. The plasma density and the electron temperature are measured by Thomson scattering 17 mm in front of the plasma terminating surface (endplate) [17]. The experiments were conducted with $B = 0.4$ T leading to $(1.5-2.5)\times10^{20}$ m^{-3} and $0.25-0.4$ eV at the plasma column center. Despite the fact that Pilot-PSI can produce much denser and slightly hotter plasmas at higher magnetic fields [18], this low field strength was preferred for the following reasons: (i) Dust recordings require the highest possible spatial resolution, which implies a short distance between the camera and the observed volume. The minimum distance is mainly determined by the maximum value of the stray magnetic field that can be tolerated by cameras [10]. (ii) The analytical description of mechanical impacts is valid for solid bodies. Dense hot plasmas increase the possibility of formation of W droplets, whose impacts cannot be described by analytical models. Droplet impacts would be nearly indistinguishable from dust impacts and pollute the datasets. (iii) The restitution curves exhibit a size dependence, hence it is essential for model validation that the dust size range is narrow and known a priori. When embedded in hot dense plasmas, W dust can enter regimes of strong vaporization.

Targets & exposure. The in-plasma mechanical impacts of dust grains on planar W targets were analyzed. The targets were circular disks of 30 mm diameter and 1 mm thickness. Mirror polishing significantly reduced some experimental uncertainties: (i) the low surface roughness ensured that the tangential and normal directions with respect to the impact plane were identical for all observed collisions, (ii) the reflection of the dust thermal radiation from the target was visible and led to an accurate identification of the impact point. In most experiments, the W target was mounted on the endplate and exposed with its surface normal parallel to the magnetic field, in a such configuration most observed impacts were close to normal $\bar{\theta} \simeq 20°$. In few experiments, the W target was mounted on a specially designed oblique holder (that was fixed on the endplate) and exposed with its surface tangent 10° with respect to the magnetic field, in such a configuration most observed impacts were close to tangential $\bar{\theta} \simeq 60°$. In both configurations, the endplate was floating. Finally, post exposure, most targets were analyzed by SEM to identify sticking events and analyze the morphology of adhered grains.

Dust injection & trajectories. Spherical W and Mo dust with nominal size distributions $5-25\,\mu$m and $15-45\,\mu$m (diameter) were supplied by TEKNA Advanced Materials. The SEM analysis of the original distributions revealed the presence of smaller grains, down to $\sim 3\,\mu$m for W and down to $\sim 10\,\mu$m for Mo. Sub-populations with narrower size distributions were generated via meshing. The size ranges of the three sub-populations employed in these experiments were $8-10\,\mu$m for W (with a $9\,\mu$m most probable diameter), $12-16\,\mu$m for W ($14\,\mu$m most probable) and $12-16\,\mu$m for Mo ($14\,\mu$m most probable). Dust was injected from the top of the device by an electrically driven piezo-crystal dispenser. The dust dropper was installed in the middle top beam port at a height 1.875 m above the chamber axis (that coincides with the plasma column center) and an axial distance 32 cm from the endplate. According to MIGRAINe simulations, confirmed by camera observations, the injected dust, that gets charged once in the plasma, is promptly expelled from the limited-extent rotating column due to the combined effect of the ion drag

force and gravity [9]. Consequently, dust reaches the target after multiple impacts with the stainless steel vessel, passing several times through the plasma column [9, 10].

Camera arrangement & tracking. We shall only provide a brief account of the optical system and the dust tracking algorithm, for details the reader is addressed to Ref.[10]. Two high-speed visible range cameras were employed for the observation of a small volume in front of the planar W target. The side camera provided a view parallel to the surface, it was equipped with a set of lenses which led to an unprecedented spatial resolution of $6.5-9\,\mu$m/px. The temporal resolution was $33\,\mu$s. The front camera had a spatial resolution of $66-150\,\mu$m/px. The recorded videos were analysed with the TRACE code [19], which processes high speed videos, detects pinpoint bright events, classifies and arranges them into trajectories.

Uncertainties. Inherent experimental uncertainties are connected with the finite spatial and temporal resolution. Assuming that the mechanical contact is initiated at T and given that the impact duration for our size and speed range is $\delta T \sim 10\,$ns, the actual impact and rebound velocities will be $\boldsymbol{v}_{\rm inc} = \boldsymbol{v}(T)$, $\boldsymbol{v}_{\rm reb} = \boldsymbol{v}(T+\delta T)$. The experimental velocities cannot be extracted within such a short interval implying a contamination by acceleration due to plasma forces. An estimate of their effect is not possible, due to the lack of theoretical expressions valid in the proximity of the sheath. However, we consider that the uncertainty is small given that the unresolved length is a small fraction of the overall acceleration length. Additional uncertainties arise when comparing with theoretical predictions: (i) Provisions had been taken to prevent the injection of small agglomerates, which do not always break up when embedded in the plasma. A fine $19\,\mu$m square cell mesh was installed at the bottom of the dust dropper in order to reduce the number of agglomerates by limiting the possible orientations that can geometrically escape. This did not eliminate the problem, post-mortem SEM analysis of the targets revealed that the stuck grains were often doublets. Small agglomerates have an effective size much larger than the expected and, more important, they do not abide by the T&N restitution curve mainly due to their non-spherical shape and the possibility of spinning. (ii) The injected dust size distributions are narrow but not monodisperse. The T&N restitution curves have a direct size-dependence through the adhesive velocity and an indirect through the yield strength. The related uncertainty is straightforward to compute and has been considered. (iii) The injected dust grains follow different paths inside the plasma which results to different bulk temperatures at the instant of the collision. The temperature dependence of the relevant mechanical properties $(E^*, \gamma, \rho_{\rm d}, \sigma_{\rm y})$ implies an uncertainty in the T&N restitution curves. For our W size distribution, provided that the bulk dust temperature exceeds 1500 K, the associated uncertainty is very small. (iv) Omnipresent nano-roughness in both the dust grains and the planar targets can significantly modify the very low velocity limit of the restitution curves. Its effect has been incorporated in MIGRAINe by randomizing the adhesive velocity from zero to its nominal JKR value. It is probably responsible for the strong fluctuations observed in the low speed range of the experimental restitution curves.

4. Experimental results

Micrometer sphere experiments are notoriously hard to perform. Even controlled room-temperature experiments with centimeter spheres are characterized by uncertainties in the restitution coefficients [15], despite the fact that they are not influenced by agglomerate, size, temperature or roughness-related uncertainties. Experiments with micron dust impacts naturally occurring in fusion relevant environments will unavoidably result in strongly fluctuating restitution curves. Therefore, large impact statistics as well as experiments with varying material characteristics and plasma conditions are required. Six different measurement sets were obtained and 520 impacts were analyzed.

Experimental dataset #1. Spherical W dust $8-10\,\mu$m in diameter was injected in six discharges with $B = 0.4\,$T, $I = 220\,$A, 2.5 slm hydrogen gas flow rate, 2 s duration. The planar W target of $R_{\rm q} = 35\,$nm surface roughness was exposed normally. At the plasma column center, above the target, the electron temperature and density were 0.4 eV and $2.5\times10^{20}\,$m^{-3}. The resolution of the front and side cameras was 100 and $9\,\mu$m/px, respectively. From the trajectories recorded, 230 impacts were suitable for the video analysis featuring 62 sticking events and 168 inelastic rebounds. The normal impact speeds were in the $1.36-12.95\,$m/s range, the tangential impact speeds in the $0-6.88\,$m/s range and the impact angles in the $0^\circ-73.4^\circ$ range with an average of 24.3°. Concerning the normal component of the collision, 119 impacts corresponding to $\sim 71\%$ were accompanied by strong dissipation of the normal velocity with their normal restitution coefficients $e_\perp < 0.6$, whereas the remaining 49 impacts were characterized by $e_\perp > 0.6$. Concerning the tangential component, all impacts were accompanied by weak dissipation of the tangential velocity, the tangential restitution coefficient always exceeded 0.61 with an average value $\bar{e}_\parallel = 0.86$. The restitution coefficients are plotted in Fig.1 and Fig.2.

Experimental dataset #2. W dust $8-10\,\mu$m was injected in one 2 s discharge: $B = 0.4\,$T, $I = 220\,$A, 2.5 slm. The planar W target of $R_{\rm q} = 27\,$nm was exposed normally. The plasma column is expected to be slightly weaker than in the previous experiment, since there were evidence of degradation of the cascaded arc source. The front and side camera resolution was 66 and $6.5\,\mu$m/px, respectively. 65 impacts were suitable for the analysis featuring 9 sticking events and 56 inelastic rebounds. The normal and tangential impact speeds were $0.70-8.86\,$m/s and $0-3.53\,$m/s, the impact angles $0^\circ-73.3^\circ$ with a 22.9° average. 37 impacts corresponding to $\sim 66\%$ were accompanied by strong dissipation of the normal velocity with $e_\perp < 0.6$ (see Fig.3), whereas the remaining 19 impacts were characterized by $e_\perp > 0.6$. Nearly all impacts were accompanied

by weak dissipation of the tangential velocity, the average tangential restitution coefficient was $\bar{e}_{\|} = 0.75$.

Experimental dataset #3. W dust $8 - 10\,\mu$m was injected in two 2 s discharges: $B = 0.4\,$T, $I = 130 - 150\,$A, 2.5 slm. The planar W target of $R_q = 27\,$nm was exposed normally. At the plasma column center, above the target, the electron temperature and density were 0.25 eV and $1.5 \times 10^{20}\,$m^{-3}. The front and side camera resolution was 66 and 6.5 μm/px, respectively. 122 impacts were suitable for the analysis featuring 2 sticking events and 120 inelastic rebounds. The normal and tangential impact speeds were $0.78 - 7.71\,$m/s and $0 - 3.11\,$m/s, the impact angles $0^\circ - 80.8^\circ$ with a 19.0° average. 90 impacts corresponding to 75% were accompanied by strong dissipation of the normal velocity with $e_\perp < 0.6$ (see Fig.4), whereas the remaining 30 impacts were characterized by $e_\perp > 0.6$. Nearly all impacts were accompanied by weak dissipation of the tangential velocity, the average value of the tangential restitution coefficient was $\bar{e}_{\|} = 0.83$.

Experimental dataset #4. W dust $8 - 10\,\mu$m was injected in two 2 s discharges: $B = 0.4\,$T, $I = 220\,$A, 2.5 slm. The planar W target of $R_q = 40\,$nm was exposed obliquely. The plasma column was weaker than in the previous experiments due to the insertion of the mechanical support. The front and side camera resolution was 150 and 6.5 μm/px. 41 impacts were suitable for the analysis, no sticking event was observed. The normal and tangential impact speeds were $0.88 - 4.50\,$m/s and $2.04 - 8.81\,$m/s, the impact angles $42.9^\circ - 77.3^\circ$ with a 60.6° average. All impacts were accompanied by strong dissipation of the normal velocity with $e_\perp < 0.6$ (see Fig.5) and weak dissipation of the tangential velocity. The tangential restitution coefficient always exceeded 0.56 with $\bar{e}_{\|} = 0.74$.

Experimental dataset #5. Spherical W dust $12 - 16\,\mu$m was injected in two 2 s discharges: $B = 0.4\,$T, $I = 220\,$A, 2.5 slm. The planar W target of $R_q = 30\,$nm was exposed normally. At the plasma column center, above the target, the electron temperature and density were 0.4 eV and $2.5 \times 10^{20}\,$m^{-3}. The front and side camera resolution was 66 and 6.5 μm/px. 49 impacts were suitable for the analysis featuring 2 sticking events and 47 inelastic rebounds. The normal and tangential impact speeds were $0.57 - 7.90\,$m/s and $0 - 2.48\,$m/s, the impact angles $0^\circ - 57.8^\circ$ with a 21.7° average. 37 impacts corresponding to $\sim 79\%$ were accompanied by strong dissipation of the normal velocity with $e_\perp < 0.6$ (see Fig.6), whereas the remaining 10 impacts were characterized by $e_\perp > 0.6$. Nearly all impacts were accompanied by weak dissipation of the tangential velocity, the average value of the tangential restitution coefficient was $\bar{e}_{\|} = 0.76$.

Experimental dataset #6. Mo dust $12 - 16\,\mu$m was injected into two 5 s discharges: $B = 0.4\,$T, $I = 220\,$A, 2.5 slm hydrogen flux, $T_e = 0.4\,$eV, $n = 2.5 \times 10^{20}\,$m^{-3}. The planar W target of $R_q = 32\,$nm was exposed normally. Only 13 impacts were recorded by the lower resolution front camera, all resulting to sticking.

Tangential restitution coefficient for all impacts. The

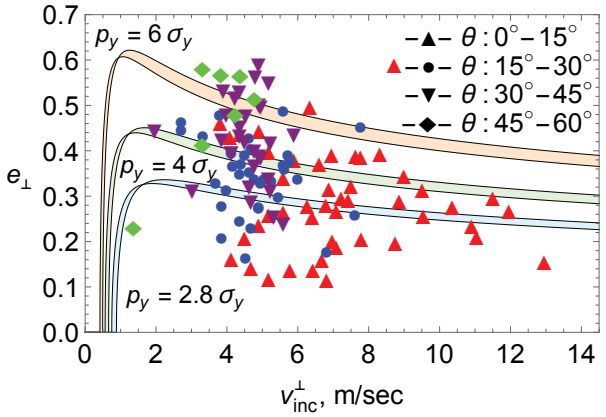

Figure 1: Dataset #1, strong normal dissipation: the experimental normal restitution coefficient as a function of the normal impact velocity. The continuous curves correspond to the T&N model, Eq.(3), for various input values of the limiting pressure. The temperature and size dependence of the mechanical properties has been taken into account, $T_d = 3000\,$K and $T_t = 1000\,$K was assumed for the temperatures of the dust grain and the target, respectively. For each p_y different T&N curves were produced for $R_d = 4\,\mu$m and $R_d = 5\,\mu$m due to the poly-disperse nature of the injected dust population ($8 - 10\,\mu$m in diameter). The theoretical result is represented by the (shadowed) area between the curves.

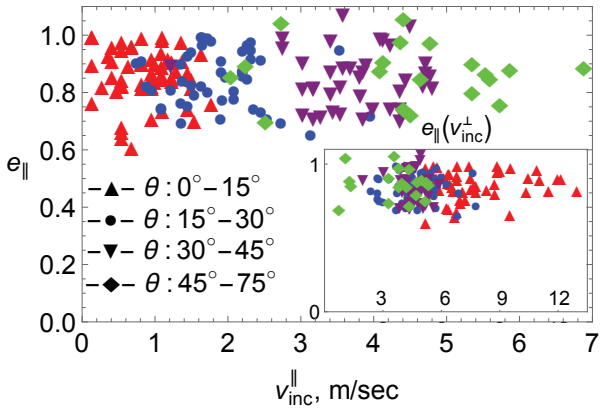

Figure 2: Dataset #1, all impacts: the experimental tangential restitution coefficient as a function of the tangential impact velocity (main plot) and as a function of the normal impact velocity (insert).

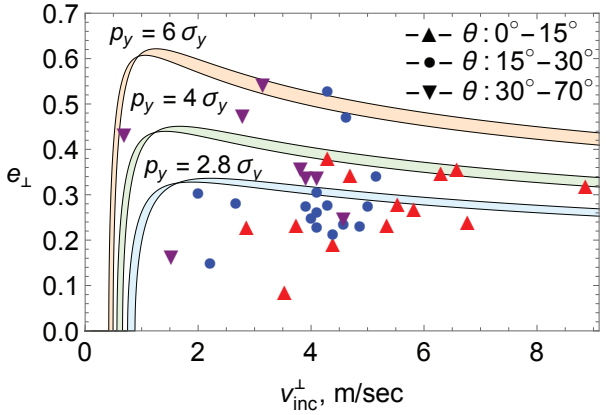

Figure 3: Dataset #2, strong normal dissipation. See the caption of Fig.1 for details.

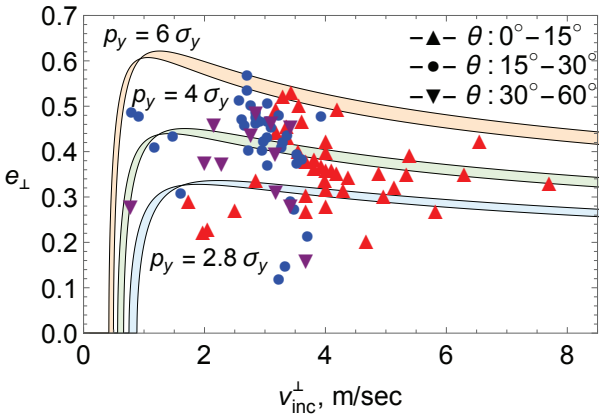

Figure 4: Dataset #3, strong normal dissipation. See the caption of Fig.1 for details.

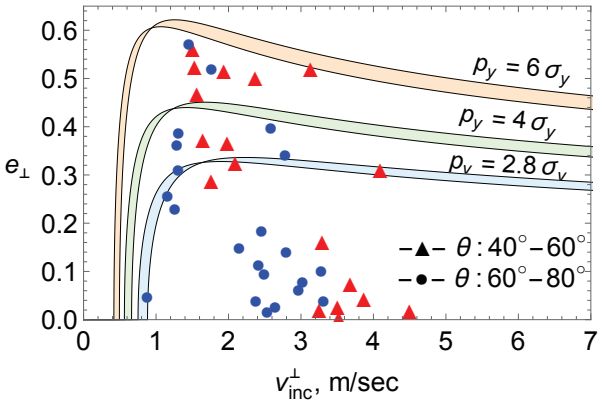

Figure 5: Dataset #4, all impacts. See the caption of Fig.1.

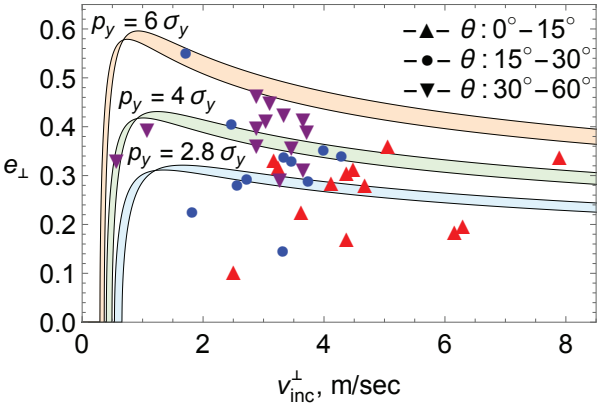

Figure 6: Dataset #5, strong normal dissipation. For each p_y different T&N curves were produced for $R_{\rm d} = 6\,\mu$m and $R_{\rm d} = 8\,\mu$m due to the poly-disperse nature of the injected dust population ($12 - 16\,\mu$m in diameter). See also the caption of Fig.1 for details.

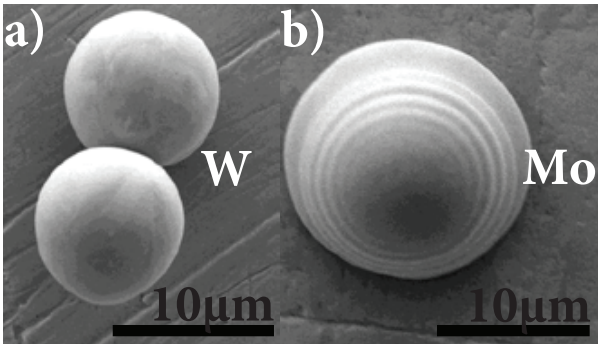

Figure 7: SEM images of dust grains stuck on the planar W target: a) W doublet from dataset #2, b) molten Mo grain from dataset #6.

measurements confirm that frictional dissipation is much less than adhesive and plastic dissipation. Datasets #2 – 5 display an identical behavior to dataset #1, the latter depicted in Fig.2. The tangential restitution coefficient is nearly independent of the normal and tangential components of the impact velocity. It exhibits small fluctuations around a mean value that slightly differs between the datasets. The approximation $e_{\parallel} = 0.8$ is an adequate representation of the measurements that is more accurate than the current MIGRAINe assumption $e_{\parallel} = 1$ [3].

Normal restitution coefficient for near-normal impacts. These events correspond to datasets #1, 2, 3, 5. The majority of impacts $\sim 75\%$ was characterized by strong normal dissipation, their agreement with the T&N model is reasonable, provided that $p_{\rm y} \simeq 4\sigma_{\rm y}$ is employed for the limiting contact pressure. The MIGRAINe value of $p_{\rm y} = 2.8\sigma_{\rm y}$ [6] appears to overestimate the normal dissipation, see Figs.1,3,4,6. On the other hand, $\sim 25\%$ of the impacts was characterized by weak normal dissipation and cannot be described by the T&N model. Three mechanisms can be responsible for the reduced normal dissipation: nano-roughness reduces adhesive work [20], spinning enables energy transfer from rotational to translational degrees of freedom [21], agglomerate impact introduces physics beyond the T&N model. These are speculations and it has not been possible to conclusively demonstrate whether any of these mechanisms becomes effective. However, SEM evidence point towards agglomerate impacts (see below).

Normal restitution coefficient for near-tangential impacts. These events correspond to dataset #4, illustrated in Fig.5. For oblique impacts, the T&N model significantly overestimates the normal restitution coefficient. The deviations increase as the normal component of the impact velocity increases. This observation agrees with other works, where it was concluded that $e_\perp$ depends only on the normal impact velocity for impact angles $\lesssim 45^\circ$, whereas for near-tangential impacts $e_\perp$ also depends on the impact angle [22, 23]. In particular, these works suggested that $e_\perp(\theta = 0)/e_\perp(\theta \gtrsim 45^\circ) > 1$ and that the ratio increases as the normal component of the impact velocity increases.

Sticking events. For the experiments corresponding to datasets #2 – 6, a post-mortem SEM analysis of the planar W target was carried out. (i) The adhered W dust grains never displayed any macro-morphological changes, supporting our estimate that W dust does not melt at $B = 0.4\,$T. (ii) A small fraction of the W dust grains was adhered as doublets. Judging from the rarity of the sticking events and the large surface of the target, it is highly

unlikely that the doublet was formed by two independent sticking impacts, implying that part of the injected dust population involved small agglomerates that did not break up in the plasma. An example is illustrated in Fig.7a, only one of the grains is in contact with the target. (iii) A fraction of the adhered Mo grains had clearly re-solidified, the formation of droplets is consistent with the observation that all Mo impacts captured by the cameras were accompanied by sticking. An example is depicted in Fig.7b, the morphology can be roughly explained by considering that the target is much colder ($\lesssim 1000\,\mathrm{K}$) than the droplet ($> 2900\,\mathrm{K}$) [24]: At the initial stage of the impact, the Mo droplet flattened into a disk and a re-solidified layer formed at the interface. The upper layer remained liquid and started to recoil, but this backward flow was counteracted by cohesion. After a number of oscillations, the solidification front caught up.

5. Summary and conclusions

Dust injection experiments have been carried out in Pilot-PSI focusing on the visualization of *in-plasma* mechanical collisions of W dust on W surfaces with an unprecedented resolution. Large statistics and careful reduction of the various unavoidable experimental uncertainties allowed for a calibration of certain aspects of the impact model that is implemented in the MIGRAINe dust dynamics code: (i) An empirical value is determined for the ratio of the limiting contact pressure over the yield strength of dust. This ratio controls plastic dissipation and thus the normal restitution coefficient. The approximate empirical value 4 is close to the theoretical value 2.8 previously employed in MIGRAINe. (ii) It is demonstrated that the parallel restitution coefficient is nearly independent of both the normal and the tangential components of the impact velocity. Its average value 0.8 is close to the value 1 previously employed in MIGRAINe. (iii) The T&N model of normal impact is shown to lead to a significant underestimation of the dissipation for near-tangential impacts. This has also been concluded by earlier theoretical works. (iv) It is suggested that a major source of systematic deviations from the T&N model is agglomerate injection. These do not fully break up inside the plasma and collide as small agglomerates (doublets) contaminating the dataset.

Acknowledgments

The authors would like to thank G. Riva and G. Daminelli for the target and dust preparation, as well as D. Ripamonti for the SEM analysis. This work has been carried out within the framework of the EUROfusion Consortium and has received funding from the Euratom research and training programme 2014-2018 under grant agreement No 633053. Work performed under EUROfusion WP PFC. The views and opinions expressed herein do not necessarily reflect those of the European Commission.

[1] S. I. Krasheninnikov, R. D. Smirnov and D. L. Rudakov, *Plasma Phys. Control. Fusion* **53** (2011) 083001.
[2] S. Ratynskaia, C. Castaldo, H. Bergsåker and D. Rudakov, *Plasma Phys. Control. Fusion* **53** (2011) 074009.
[3] S. Ratynskaia, L. Vignitchouk, P. Tolias, I. Bykov *et al.*, *Nucl. Fusion* **53** (2013) 123002.
[4] D. L. Rudakov, A. Litnovsky, W. P. West, J. H. Yu *et al.*, *Nucl. Fusion* **49** (2009) 085022.
[5] A. Shalpegin, L. Vignitchouk, I. Erofeev, F. Brochard *et al.*, *Plasma Phys. Control. Fusion* **57** (2015) 125017.
[6] L. Vignitchouk, P. Tolias and S. Ratynskaia, *Plasma Phys. Control. Fusion* **56** (2014) 095005.
[7] C. Thornton and Z. Ning, *Powder Technol.* **99** (1998) 154.
[8] D. A. Gorham and A. H. Kharaz, *Powder Technol.* **112** (2000) 193.
[9] S. Ratynskaia, P. Tolias, A. Shalpegin, L. Vignitchouk *et al.*, *J. Nucl. Mater.* **463** (2015) 877.
[10] A. Shalpegin, F. Brochard, S. Ratynskaia, P. Tolias *et al.*, *Nucl. Fusion* **55** (2015) 112001.
[11] K. L. Johnson, K. Kendall and A. D. Roberts, *Proc. R. Soc. A* **324** (1971) 301.
[12] P. Tolias, S. Ratynskaia, M. De Angeli, G. De Temmerman *et al.*, *Plasma Phys. Control. Fusion* **58** (2016) 025009.
[13] L.-Y. Li, C.-Y. Wu and C. Thornton, *Proc. Inst. Mech. Eng. C* **216** (2002) 421.
[14] C.-Y. Wu, L.-Y. Li and C. Thornton, *Int. J. Impact Eng.* **28** (2003) 929.
[15] A. B. Stevens and C. M. Hrenya, *Powder Technol.* **154** (2005) 99.
[16] G. De Temmerman, J. J. Zielinski, S. van Diepen, L. Marot and M. Price, *Nucl. Fusion* **51** (2011) 073008.
[17] H. J. van der Meiden, R. S. Al, C. J. Barth, A. J. H. Donné *et al.*, *Rev. Sci. Instrum.* **79** (2008) 013505.
[18] G. J. van Rooij, V. P. Veremiyenko, W. J. Goedheer, B. de Groot *et al.*, *Appl. Phys. Lett.* **90** (2007) 121501.
[19] S. Bardin, J.-L. Briancon, F. Brochard, V. Martin *et al.*, *Contrib. Plasma Phys.* **51** (2011) 246.
[20] D. Tabor, *J. Colloid Interface Sci.* **58** (1977) 2.
[21] H. Dong and M. H. Moys *Powder Technol.* **161** (2006) 22.
[22] C.-Y. Wu, C. Thornton and L.-Y. Li, *Adv. Powder Technol.* **14** (2003) 435.
[23] C.-Y. Wu, C. Thornton and L.-Y. Li, *Proc. R. Soc. A* **465** (2009) 937.
[24] M. Pasandideh-Fard, S. Chandra and J. Mostaghimi, *Int. J. Heat Mass Transfer* **45** (2002) 2229.